

Experimental Study of Flying and Contact Dynamics of an Al₂O₃-TiC Slider with a Piezoelectric Nanoactuator

Jia-Yang Juang, Rohit P. Ambekar and David B. Bogy

Computer Mechanics Laboratory
Department of Mechanical Engineering
University of California at Berkeley
Berkeley, CA 94720

C. Singh Bhatia

Hitachi GST
5600 Cottle Road
San Jose, CA 95193

ABSTRACT

In this report we designed and fabricated Al₂O₃-TiC sliders with a special ABS design and a piezoelectric actuator for achieving high actuation efficiency. We fabricated and assembled prototype sliders using an inexpensive and low-temperature process. The measured nonflying actuated stroke exhibited a linear relationship with the applied voltage with a rate of ~ 0.8 nm/V. The FHs of two different sliders, designed for the actuated center pad and actuated side pads schemes, were successfully reduced from 15.5 nm and 8.5 nm to contact with applied voltages of 20 V and 10 V, respectively, which demonstrated high actuation efficiency. The AE measurements showed clear spikes when the center pad was brought into contact with the disk by the actuator. The pattern of the AE signals during contact is different from the one observed in the conventional sliders during “touchdown-takeoff tests” where there is a pronounced increase in the AE amplitude upon contact. This is attributed to the sustained air bearing even when the intermittent contacts occur in the head-

disk interface. It is also found that the dominant air bearing mode shifted from the first pitch to the second pitch as a result of the intermittent contacts. In addition, a track of considerable lube depletion and carbon wear was observed after the contact tests.

1. INTRODUCTION

As the spacing between the slider and the disk decreases in hard disk drives the linear bit spacing of the magnetic recording can decrease, resulting in a higher areal density. A gap flying height of less than 5 nm between the read/write element and the surface of the disk is required for ultrahigh density recording. A stable and constant FH must also be sustained in the presence of altitude and temperature changes, manufacturing tolerance, and track-seeking motion. Furthermore, the dynamic instability caused by FH modulations (FHMs) and nanoscale adhesion forces, such as electrostatic and intermolecular forces, should be minimized. Those challenges make a conventional air bearing surface (ABS) slider an unlikely choice for an areal density of 1 Tbit/in². One potential solution is a FH adjustment or control slider that is capable of adjusting its gap FH with sub-nanometer resolution.

Due to its quick response and low power consumption piezoelectric materials have been proposed as active elements for adjusting the FH. Yeack-Scranton *et al.* [1] proposed an active slider for contact recording, where a piezoelectric material was inserted in a channel that ran across the full width of the slider at its top rear. They experimentally demonstrated movement of the read/write element from ~ 200 nm to contact, but the proposed structure of piezoelectric actuator is difficult to implement in the smaller currently used pico- or femto-sized sliders. Another approach is to bond a layer of piezoelectric material to one side of the suspension and change the FH by bending the suspension [2], [3]. The bandwidth of actuation is limited by that of the suspension dynamics, which is much lower than that of the air bearing. Khanna *et al.* [4] in 1991 and then Zhang *et al.* [5] in 2005 reported a method of FH adjustment by bonding a bulk piezoelectric material on the backside of a slider body. The FH was adjusted by applying a voltage to the piezoelectric material and thereby changing the

crown and/or camber of the slider body. The structure of such sliders is simpler and it is relatively easy to fabricate, but the fact that the FH is adjusted by changing the crown and/or camber contradicts the ABS design rule of reducing sensitivity of flying attitudes to these two parameters. Another approach is to utilize piezoelectrically actuated unimorph cantilever sliders. Several papers, such as Kurita *et al.* [6], [7], Tagawa *et al.* [8], Suzuki *et al.* [9], and Su *et al.* [10], have presented active sliders made of silicon with piezoelectric unimorph cantilevers. The slider structure was simpler and could be fabricated by silicon microfabrication technology. However, the use of silicon as the slider material and the requirement of high temperature processes make it difficult to integrate with current fabrication technology. Juang *et al.* [11] developed a low-temperature and inexpensive process for fabricating and integrating Al₂O₃-TiC sliders with piezoelectric nanoactuators using a conventional ABS. They found that the actuation efficiency was only 7 % due to the strong counter effect of the air bearing.

In this report we designed and fabricated Al₂O₃-TiC sliders with a special ABS design and a piezoelectric actuator for achieving high actuation efficiency. Experiments using a Zygo optical profiler, dynamic FH tester (DFHT), acoustic emission sensor (AE), laser Doppler vibrometer (LDV) and optical surface analyzer (OSA) were carried out to study the actuation and flying performance as well as the slider dynamics when the center pad is actuated to contact the disk.

2. EXPERIMENTS

A schematic diagram of the controlled-FH slider with an unimorph piezoelectric nanoactuator is shown in Fig. 1. The slider carries a layer of piezoelectric material, which is located between the slider body and the suspension flexure. The two slits near the trailing

edge are created to form a cantilever. The piezoelectric layer is separated into three parts by a dicing process. The read/write element is located on the air bearing surface near the end of the cantilever. There are two operational schemes: actuated center-pad and actuated side-pads. For the actuated center-pad scheme, an electric voltage is applied to the middle portion of the piezoelectric material and the cantilever bends down or up depending on the polarity of the induced electric field, resulting in a decrease or increase of the gap FH. For the actuated side-pads scheme, an electrical voltage is applied to the piezoelectric layers on the two sides and the FH is reduced when the two side-pads are bended up, causing a relative downward displacement of the center pad with respect to the ABS. According to the sign convention in this study, a positive stroke is the one that reduces the FH and vice versa.

An ABS design named Scorpion is used in this study. As illustrated in Fig. 2(a) it has four levels of etching steps and was designed for piezoelectric sliders with high air bearing stiffness and damping [12]. The targeted gap FH (without actuation) is 12 nm at a disk velocity of 15000 rpm. Fig. 2 (b) shows the pressure distribution of the Scorpion ABS. Instead of being supported by the center pressure peak the slider is primarily supported by the high pressures generated at the side trailing pads, which significantly increases the actuation efficiency (defined as the ratio of the FH reduction to the stroke). The two white rectangles are slits that run through the entire slider thickness and have dimensions of $65 \times 600 \mu\text{m}$.

The fabrication process of Al_2O_3 -TiC sliders with piezoelectric actuators developed in [11] was used in this study. The process starts from dicing wafers into quads and cutting them into row-bars, followed by lapping of the row-bars to the desired slider thickness. The ABS is then defined and etched by photolithography and dry-etch processes such as ion-

milling and reactive-ion etching. A thin layer of diamond-like carbon (DLC) is deposited on the entire ABS to protect the read/write element from corrosion and wear. The row-bars are then bonded with 127- μm thick commercially available lead-zirconate-titanate (PZT) sheets (Piezo Systems, Inc.) by silver epoxy (Transene Company, Inc.). Thin vacuum sputtered nickel electrodes have been deposited on both surfaces of the PZT sheets to produce extremely low current leakage and low magnetic permeability. A standard dicing process is used to separate the PZT and to cut the row-bars into individual sliders. Since there are no deep reactive-ion etching or high temperature processes involved the cost introduced by these additional steps can be kept at a minimum, and the previously deposited read/write element will not be damaged. The sliders are then mounted onto suspensions by the use of conductive and nonconductive glues to complete the suspension-gimbal assembly (HGA). The electrodes on the suspension flexure for read/write heads are used to apply voltages to the actuator. An example of the fabricated Al_2O_3 -TiC sliders with a layer of PZT is shown in Fig. 3. Two prototypes Slider #1 and Slider #2 were assembled and studied for the actuated center pad and side-pads scheme, respectively.

These tests were conducted on a Candella OSA spinstand, with a dual-channel LDV for monitoring slider dynamics and AE sensor for detecting contact. One channel of the LDV was focused on the slider back and measured the slider velocity in the Z-direction. This was integrated to obtain the slider displacement over time. To capture the repeatable part of the slider displacements the second channel of the LDV was used as a trigger to the data acquisition system which averaged the slider velocity channel accurately over 300 disk revolutions. The trigger was obtained from a scratch on the disk edge, which gives a very

accurate trigger [13]. Three measurements of slider displacements were taken corresponding to each voltage, which was varied from 0V to 60V in steps on 10V.

A smooth disk (rms 0.2 nm) with 12Å Zdol 4000 lube was used for conducting the tests. After each voltage cycle of 0V-60V-0V, the disk was monitored for lubricant depletion.

3. RESULTS AND DISCUSSIONS

3.1 Nonflying Stroke of the Piezoelectric Nanoactuator

The unimorph actuator, composed of a piece of piezoelectric material and a portion of the slider, deflects under an electric voltage V and an external vertical force F exerted on the tip. The constitutive equation of the tip deflection subject to a voltage and a force can be described as follows [14]:

$$\delta = aF + bV \quad (1)$$

$$a = \frac{1}{k_s} = \frac{4L^3}{E_p w t_p^3} \frac{\alpha\beta(1+\beta)}{\alpha^2\beta^4 + 2\alpha(2\beta + 3\beta^2 + 2\beta^3) + 1}$$

$$b = \frac{3L^2}{t_p^2} \frac{\alpha\beta(1+\beta)}{\alpha^2\beta^4 + 2\alpha(2\beta + 3\beta^2 + 2\beta^3) + 1} d_{31}$$

$$\alpha = \frac{E_s}{E_p}, \quad \beta = \frac{t_s}{t_p}$$

where the subscripts s and p stand for the slider and piezoelectric materials, respectively. E and t are the Young's modulus and beam thickness, respectively. L and w represent the length and width of the composite beam. k_s is the bending stiffness of the cantilever. d_{31} is the piezoelectric coefficient.

According to Eq.(1) the actuated stroke as a function of the cantilever length was calculated without an external force. The thicknesses of the PZT and Al₂O₃-TiC layers are 127 and 300 μm, respectively. The material properties are $E_p = 62$ GPa, $E_s = 398$ GPa, $d_{31} = -320 \times 10^{-12}$ m/V. It is seen that the stroke increases as the actuator length increases and is about 0.6 nm/V for a length of 600-μm.

The nonflying actuated stroke of the prototype sliders at the pole-tip as a function of applied voltage was measured by a Zygo NewView interferometer (Zygo Corporation). Fig. 5 shows an example of a measurement obtained by the instrument. The topography of a portion of the slider near the trailing edge was measured and analyzed. The profile along the direction of slider width was plotted in Fig. 5(b). It is observed that there are three etching steps (four levels) with etch depths of about 191 nm, 1.38 μm and 1.88 μm. The actuation stroke was measured as the height difference between the center pad and the two side-pads when an electrical voltage is applied to the piezoelectric materials. It is noted that an initial stroke of several nanometers was observed even when no voltage was applied, which may be attributed to the cutting/bonding process and/or the mismatch of coefficients of thermal expansion of the PZT and Al₂O₃-TiC. Further investigation is required for minimizing and eliminating the initial stroke.

The actuated stroke was obtained by subtracting the initial surface profile (without voltage) from the actuated one (with voltage). Fig. 6 shows the stroke of Slider #1 when the voltage was increased from 0 to 40 V and returned to 0 V. A stroke of 32 nm was obtained at a voltage of 40 V, corresponding to a rate of 0.8 nm/V. A slight hysteresis was also observed. The measured stroke is 0.2 nm/V larger than the calculated value of 0.6 nm/V at a length of 600 μm, and it fits the calculated stroke when the actuator length is 700 μm. This result

indicates that the effective actuation length is 100 μm longer than the cutting length of the slits.

Similarly, the actuated stroke of Slider #2 was measured. The driving voltage was gradually increased from 0 to 60 V, returned to 0 V, decreased to -60 V and returned to 0 V to form a complete loop as shown in Fig. 7(a). A hysteresis of 5 nm was observed due to the relatively high driving voltage. The measurement data and a linear fit for the branch from 0 to 60 V are shown in Fig. 7 (b). The stroke is found to be proportional to the applied voltage with a rate of 0.72 nm/V. It is observed that Slider #1 and #2 have initial strokes of -6 and 0 nm, respectively, which have to be included in the FH measurements.

3.2 Flying Heights: Measurements and Simulations

We used an optical dynamic FH tester (DFHT4, KLA-Tencor Corporation) to measure the FH of the fabricated suspended sliders. In the tests the sliders were flown over a glass disk at three radial positions (ID, MD, and OD) at a rotational speed of 15000 rpm and a skew angle of 0 degree. The FHs were measured at the outer trailing pad (Point A) and the inner trailing pad (Point B). The FH at the center trailing pad was not measured since the light spot of the instrument ($\sim 30 \mu\text{m}$) was larger than the available area of the center pad. Instead of direct measurements the FHs at the center pad were estimated by averaging the FHs at the two side-pads and taking the initial stroke into account. Fig. 8 shows the measured FH of Point A at the MD as a function of degree (360 degrees per revolution). The average and standard deviation are 9.11 and 0.14 nm, respectively. The experimental results are compared with numerical ones simulated by using the CML Air Bearing Simulator as shown in Table. I. The measured values are 2 to 5 nm smaller than those obtained by simulations. Such a discrepancy may be attributed to measurement error and/or to the simulation model,

which may not be accurate under ultralow flying conditions. Based on the results, the gap FHs of Slider #1 and #2 are estimated to be 15.5 nm (9.5 nm + 6 nm) and 8.5 nm (8.5 nm + 0 nm), respectively.

3.3 Contact Tests

Contact tests were conducted on an OSA spin-stand with an AE sensor for detecting contact. Slider #1 was loaded on the disk at a radial position of 26 mm and a linear speed of 38 m/s. The slider body was grounded and an electrical voltage was applied to the top electrode of the PZT actuator. The voltage was gradually increased from 0 to 60 V at an increment of 5 V. The process was repeated at a new radial position of 25 mm. Figs. 9(a) and 9(c) show the time histories of the AE signal when no voltage was applied to the piezoelectric actuator, which indicates that the slider flew well and no contact was detected by the AE sensor. Isolated spikes were observed when a voltage of 60 V was applied to the actuator as shown in Figs. 9(b) and 9(d). These spikes were caused by the intermittent contacts of the center pad and the disk. However, such a pattern of the AE signals during contact is different from the one observed in the conventional sliders during “touchdown-takeoff tests” [15] where there was a pronounced increase in the amplitude of the AE signal upon contact. Thus, during controlled contact (as is the case here) only a small portion of the slider comes into contact with the disk while the rest of the ABS is supported by the air bearing. There is no loss of air bearing as the voltage increases to increase the intensity of contact. Due to this, the corresponding AE signal showed only an increase in the frequency of contacts but not an AE avalanche which occurs in case of conventional sliders due to complete loss of the air bearing.

Fig. 10 shows the number of hits (spikes) and estimated FH as functions of the applied voltage. The contact event that has an AE amplitude over ± 500 mV was counted as a hit. The gap FH was obtained by the measured FHs at the two side-pads and the measured initial stroke with consideration of the actuation strokes. At the radial position of 26 mm, no contact event was detected when the applied voltage was less than 20 V, corresponding to a FH of -0.5 nm and contact events were first detected when the applied voltage was increased to 25 V, corresponding to a FH of about -4.5 nm. A monotonic increase in the number of hits was observed as the voltage was increased, which indicated that the event of intermittent contacts became more frequent when the actuated stroke of the center pad was increased. It is noted that the contact was first detected at a FH between -0.5 nm and -4.5 nm, which was less than the take-off height (~ 2 nm). There are two possible reasons: one may be attributed to the AE sensor which may not be sensitive enough to detect the slight contact. The other may be the push-back lifting force generated by the center trailing pad, which may reduce the actuation stroke as compared to the case without flying. A similar trend was also observed when a second test was conducted on a new track (25 mm). It is seen that the intermittent contacts were detected at a smaller voltage (15 V). Such reduction of slider stability may be attributed to the lubricant pickup after the first test. Lubricant pickup decreases the slider's stability. Further, it also causes ABS contamination, which in turn may collect miniscule debris particles and cause wear at the head-disk interface [15].

We carried out contact tests for Slider #2 for the actuated side-pads scheme. Similarly, the contact event was detected by the AE sensor at a FH of about 0 nm. Fig. 11 shows the comparison of the nonflying strokes measured before and after the contact test, which demonstrates good repeatability of piezoelectric actuation even after contact.

3.4 Flying Height Modulation

Intermittent contacts due to increase in actuation voltage also cause a change in slider dynamics. To investigate this we measured the fly height modulation for Slider #2 as described in the previous section. From Fig.12, we see that the peak-to-peak and standard deviation (3σ) of the slider displacements gradually increased as the voltage was increased. However, the increase was not substantial and signifies a gradual increase in the slider-disk contact as the center trailing pad is lowered due to the voltage increase. The repeatability for this data was also found to be good as seen from the small error bars.

Figs. 13(a) and 13(b) show the repeatable part of the slider displacements without slider-disk contact at 0 V and during slider-disk contact at 60 V, respectively. Comparing (a) and (b) we see the increased amplitude of slider displacements. Similar to the AE measurements, the difference is not as sharp compared to a conventional slider where there is a pronounced increase in the amplitude of slider displacements upon contact due to the complete loss of air bearing.

Figs. 14(a-f) show the frequency content of slider displacements as the voltage was increased from 0 to 60 V. The CML Parameter Identification Program was used to identify the air bearing frequencies and mode shapes of the Scorpion sliders in Juang *et al.* [12]. The first pitch and the second pitch modes were found to be near 100 kHz and 200 kHz, respectively. The nodal lines shown indicate that the axes of first and second pitch modes lie near the trailing and the leading edges, respectively. Using this information, we can identify the dominant ABS frequencies in Figs. 14 (a-f). The arrows shown in Figs. 14(a) and (f) indicate the first and second pitch modes. It is seen by traversing the plots (a-f) that as the

voltage (intensity of contact) increased, the second pitch mode gradually became more dominant. This can be explained as follows:

When the slider is flying the trailing edge flies much closer to the disk compared to the leading edge. Thus, the stiffness associated with the trailing edge is much more. Thus, the modulations in the leading edge fly height due to disk forcing are much more as compared to the trailing edge due to which the slider pitch mode is close to the trailing edge. Hence, the first pitch mode is dominant when there is no slider-disk contact. As the trailing pad protrudes due to increase in voltage the trailing edge flies higher and the slider pitch is also lowered. Further, only the trailing edge gets significant forcing due to impact force. Due to this the modulations of the trailing pad are much higher as compared to the leading pad so that the second pitch mode is dominant during slider-disk contact. This hypothesis can be readily tested using the LDV to monitor the dynamics of multiple points on the slider.

From Figs. 14(a-f) we also see an increase of about 14 dB (5 times) in the peak frequency components during slider-disk contact.

FHM is defined as the difference between the slider and disk displacements, i.e. the modulation of mechanical fly height over time. During the experiments the disk was scratched during slider disk contact, due to which its topography was changed substantially. Hence, the FHM as a function of applied voltage is not reported here and further tests need to be carried out to examine the same.

3.5 Controlled Contact Effect on Lubricant

The effect of controlled contact on the lube was also monitored during the full voltage cycle 0V-60V-0V, during which the trailing pad was forced in and out of contact. When one such test was conducted substantial lube depletion was seen below the side rails and the

trailing pad, indicated by arrows in Fig. 15, which plots the average lube depletion in the radial direction. Since the trailing pad was brought into contact the depletion under it was more (5 Å) than that under the side rails (1 Å - 3 Å). Overall the depletion was relatively high due to which, when the controlled contact test was repeated the second time, there was considerable wear and a wear track was seen on the disk. Fig 16 shows the track. From the OSA analysis total lubricant depletion was seen in the dark area. This area measured about 250 μm in width, slightly wider than the cantilever width (200 μm). The central white portion in the dark area was the only place where there was only lubricant depletion and no carbon wear, while the rest of the dark area had carbon wear and the generation of debris particles. There was also considerable wear of the ABS surface as seen in Fig. 17.

More tests need to be conducted to determine the reliability of the interface during partial contact using the Scorpion IV design. It is believed that the disk showed accelerated wear due to excessive increase in voltage (60V) to the cantilever which increased the contact intensity.

4. CONCLUSIONS

This report presented experimental results of Al₂O₃-TiC sliders with piezoelectric nanoactuators. We fabricated and assembled prototype sliders using an inexpensive and low-temperature process. The measured nonflying actuated stroke exhibited a linear relationship with the applied voltage with a rate of ~ 0.8 nm/V. However, a hysteresis was observed when excessive voltages (± 60V) were applied to the piezoelectric actuators. The FHs of two different sliders were successfully reduced from 15.5 nm and 8.5 nm to contact with applied voltages of 20 V and 10 V, respectively, which demonstrated high actuation efficiency. The AE measurements showed clear spikes when the center pad was brought into contact with the

disk by the actuator. However, such a pattern of the AE signals during controlled contact is different from the one observed in the conventional sliders during “touchdown-takeoff tests” where there is a pronounced increase in the amplitude upon contact. This is attributed to the sustained air bearing even when the intermittent contacts occur in the head-disk interface. It is also found that the dominant air bearing mode shifted from the first pitch to the second pitch as a result of the intermittent contacts. In addition, a track of considerable lube depletion and carbon wear was observed after the contact tests.

ACKNOWLEDGEMENT

This study is supported by the Computer Mechanics Laboratory (CML) at the University of California, Berkeley and the Information Storage Industry Consortium (INSIC). J. Y. Juang has also been supported by The California State Nanotechnology Fellowship. The authors would like to thank T. Neumann, Y. Midori and N. Bach for the help on the fabrication, measurements and useful discussions.

REFERENCES

1. C. E. Yeack-Scranton, V. D. Khanna, K. F. Etzold, and A. P. Praino, "An active slider for practical contact recording," *IEEE Trans. Magn.*, vol. 26, pp. 2478-2483, 1990.
2. D. L. Good, J. E. Mason, and H. H. Ottesen, "Fly height servo control of read/write head suspension," U.S. Patent 5,377,058, December 27, 1994.
3. X. Liu, A. Li, W. Clegg, D. F. L. Jenkins, and P. Davey, "Head-disk spacing variation suppression via active flying height control," *IEEE Trans. Instrum. Meas.*, vol. 51, pp. 897-901, 2002.
4. V. D. Khanna, F. Hendriks, and A. P. Praino, "Programmable air bearing sliders," *IEEE Trans. Magn.*, vol. 27, pp. 5145-5147, 1991.
5. M. Zhang, S. Yu, J. Liu, and B. Liu, "Flying height adjustment by slider's air bearing surface profile control," *J. Applied Physics*, vol. 97, 10P309, 2005.
6. M. Kurita, T. Yamazaki, H. Kohira, M. Matsumoto, R. Tsuchiyama, J. Xu, T. Harada, Y. Inoue, L. Su, and K. Kato, "An active-head slider with a piezoelectric actuator for controlling flying height," *IEEE Trans. Magn.*, vol. 38, pp. 2102-2104, 2002.
7. M. Kurita and K. Suzuki, "Flying-height adjustment technologies of magnetic head sliders," *IEEE Trans. Magn.*, vol. 40, pp. 332-336, 2004.
8. K. Suzuki, R. Maeda, J. Chu, T. Kato, and M. Kurita, "An active head slider using a piezoelectric cantilever for in situ flying-height control," *IEEE Trans. Magn.*, vol. 39, pp. 826-831, 2003.
9. N. Tagawa, K.-I. Kitamura, and A. Mori, "Design and fabrication of MEMS-based active slider using double-layered composite PZT thin film in hard disk drives," *IEEE Trans. Magn.*, vol. 39, pp. 926-931, 2003.

10. L. Su, M. Kurita, J. Xu, K. Kato, K. Adachi, and Y. Miyake, "Static and dynamic characteristics of active-head sliders," *Tribol. Intl.*, vol. 38, pp. 717-723, 2005.
11. J. Y. Juang, D. B. Bogy and C. S. Bhatia, "Numerical and experimental studies of an Al_2O_3 -TiC slider with a piezoelectric nanoactuator," *2006 ASME/JSME Joint Conf. on Micromechatronics for Information and Precision Equipment*, June 21-23, Santa Clara, CA.
12. J. Y. Juang, D. B. Bogy and C. S. Bhatia, "Design and dynamics of flying height control slider with piezoelectric actuation," *ASME J. of Tribol.*, submitted for publication.
13. Q. H. Zeng, B. H. Thornton, D. B. Bogy, and C. S. Bhatia, "Flyability and flying height modulation measurement of sliders with sub-10nm flying heights," *IEEE Trans. Magn.*, vol. 37, pp. 894-899, 2001.
14. Smits, J. G. and Choi, W.-S., "The Constituent Equations of Piezoelectric Heterogeneous Bimorphs," *IEEE Trans. Ultrason., Ferroelect., Freq. Contr.*, vol. 38, no. 3, pp. 256-270, 1991.
15. R. P. Ambekar and D. B. Bogy, "Effect of slider lubricant pickup on stability at the head-disk interface," *IEEE Trans. Magn.*, vol. 41, pp. 3028-3030, 2005.

TABLE I
 COMPARISONS OF THE SIMULATED AND MEASURED FHS AT POINT A (OUTER TRAILING PAD)
 AND B (INNER TRAILING PAD). THE VALUES IN THE PARENTHESES ARE THE STANDARD
 DEVIATIONS.

	OD		MD		ID	
	Sim. (nm)	Exp. (nm)	Sim. (nm)	Exp. (nm)	Sim. (nm)	Exp. (nm)
Point A	13.31	11.64 (0.2)	13.43	10.04 (0.18)	13.11	11.01 (0.18)
Point B	13.23	8.08 (0.1)	13.60	9.11 (0.14)	13.63	8.78 (0.16)

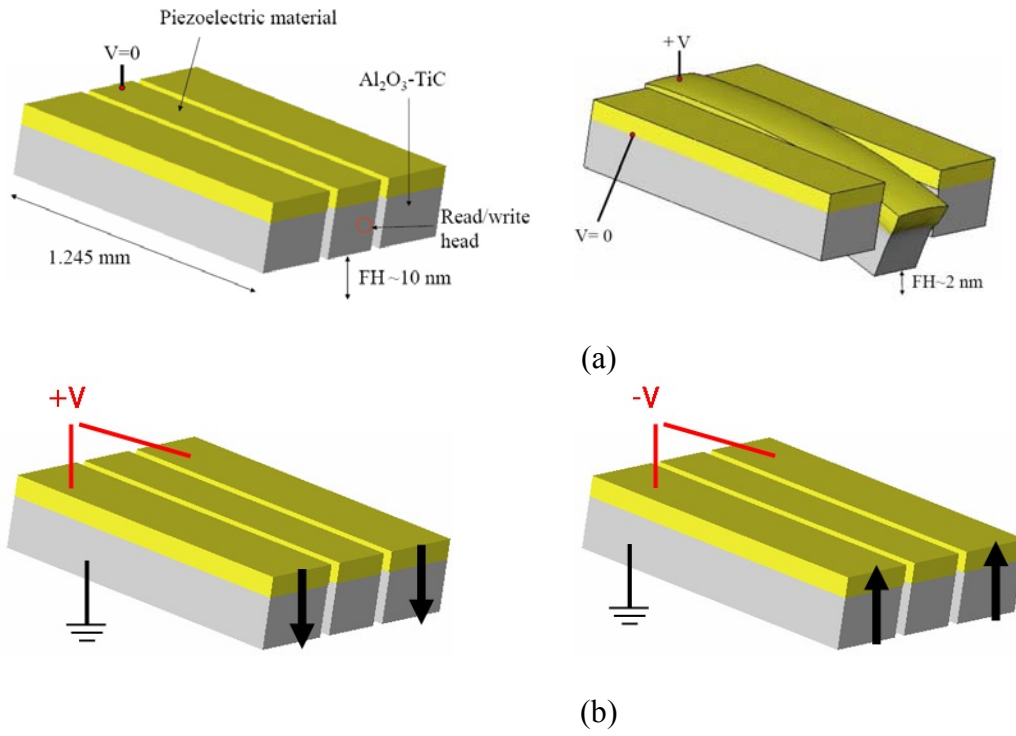
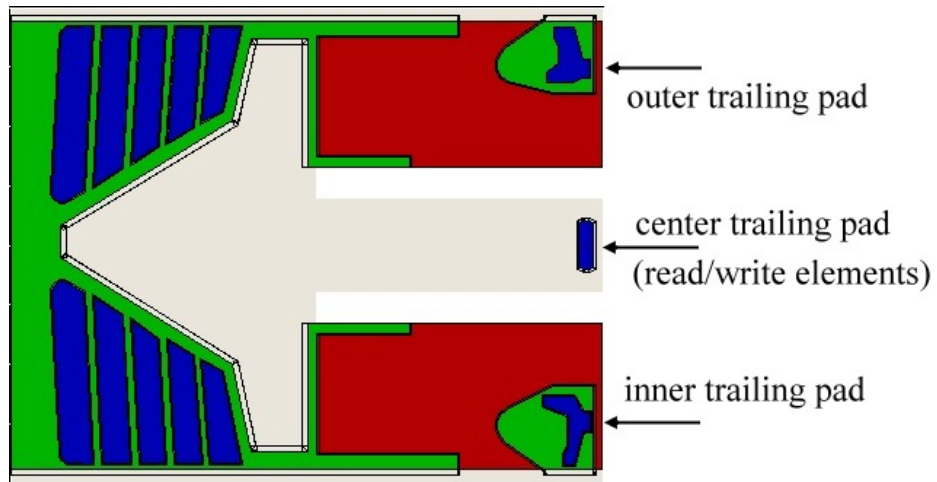
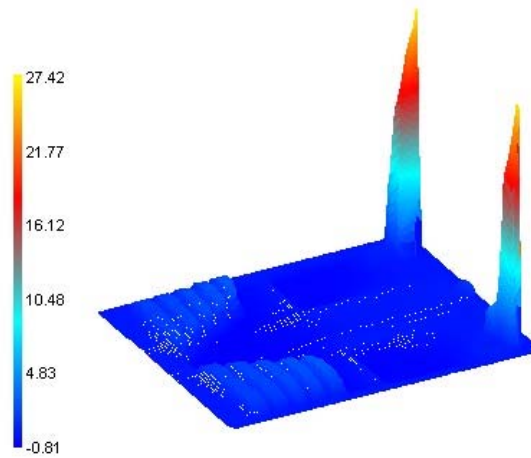


Fig. 1. Two operational schemes of a FH control slider with piezoelectric actuation. (a) actuated center-pad; (b) actuated side-pads.



(a)



(b)

Fig. 2. (a) A pico-slider ABS used in this study. The two white rectangles are slits through the entire thickness of the slider; (b) Air bearing pressure profile at radial position 29.89 mm, 0 degree skew. The scale displayed is normalized to ambient pressure: $(p - p_a)/p_a$.

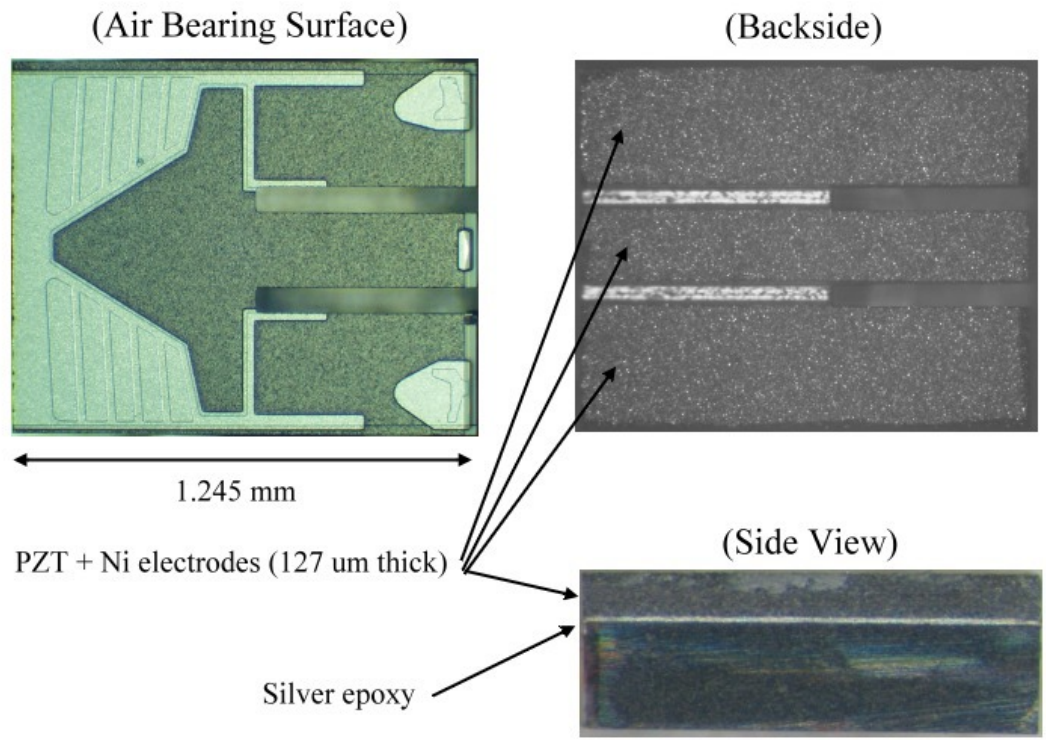


Fig. 3. Fabricated $\text{Al}_2\text{O}_3\text{-TiC}$ slider with a layer of piezoelectric material bonded on the backside.

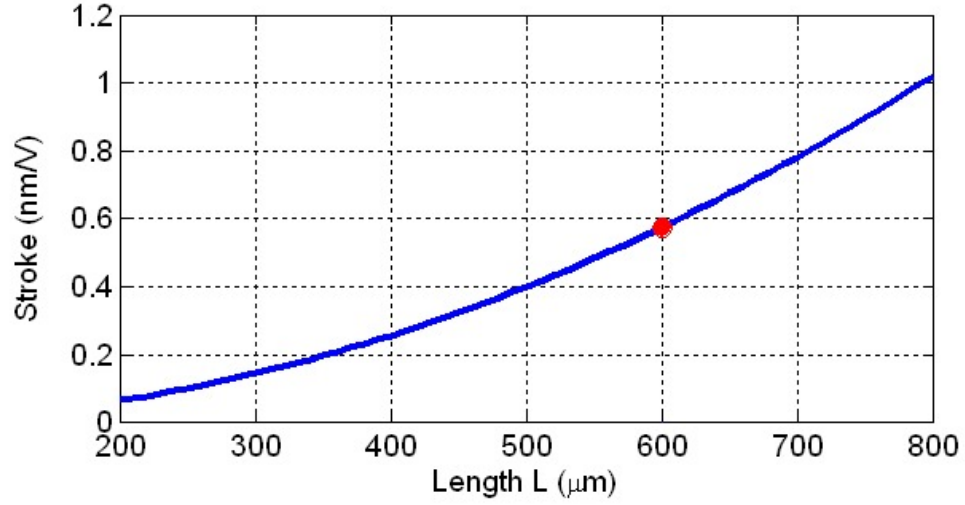
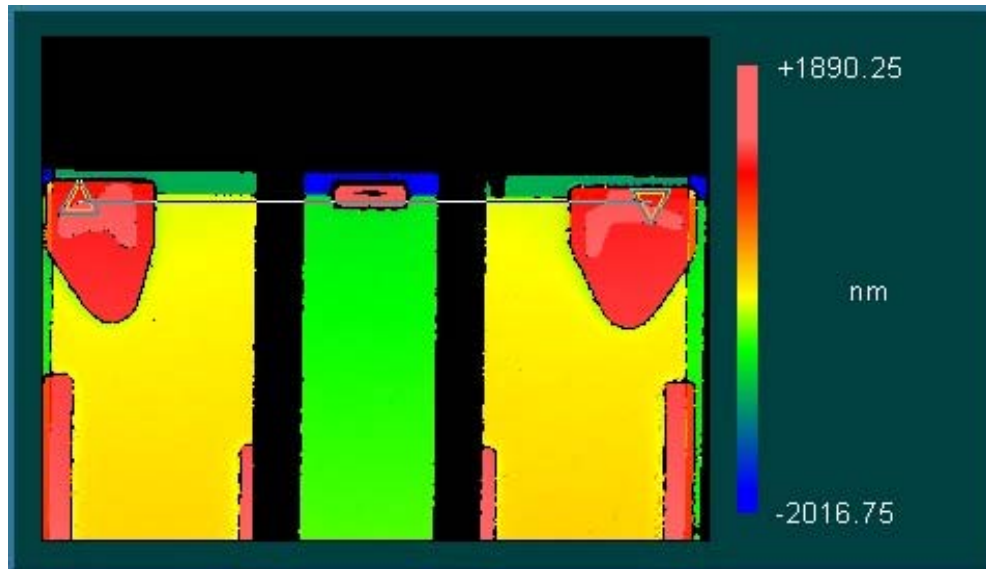
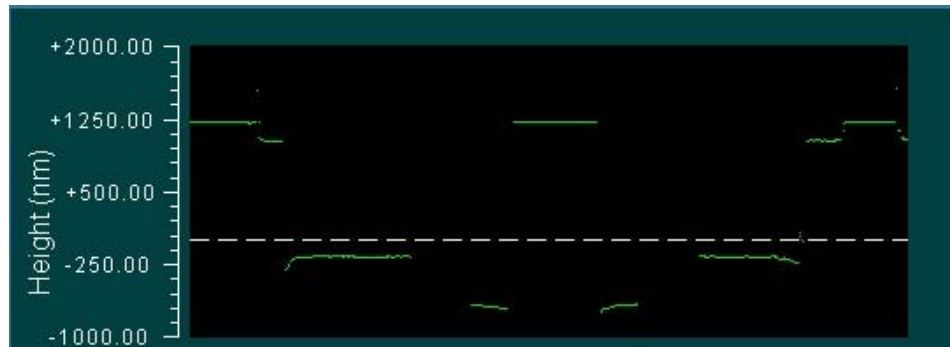


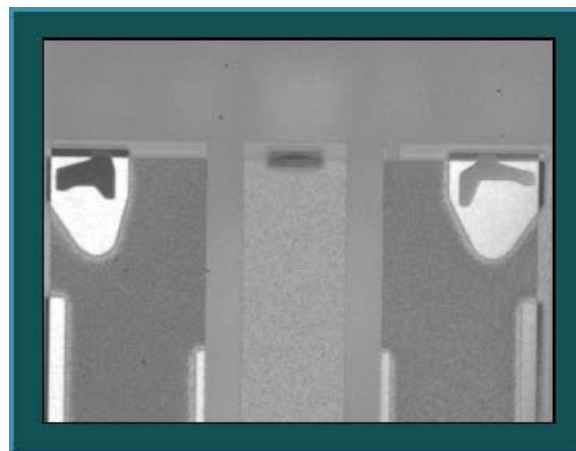
Fig. 4. The actuated stroke of a piezoelectric unimorph actuator under 1 V. The thicknesses of the piezoelectric and $\text{Al}_2\text{O}_3\text{-TiC}$ layers are 127 and 300 μm , respectively. The material properties are $E_p = 62$ GPa, $E_s = 398$ GPa, $d_{31} = -320 \times 10^{-12}$ m/V. The stroke is about 0.6 nm/V for a 600- μm long cantilever.



(a)



(b) profile



(c) Intensity data

Fig. 5. An example of an air bearing topography measured by a Zygo optical profiler.

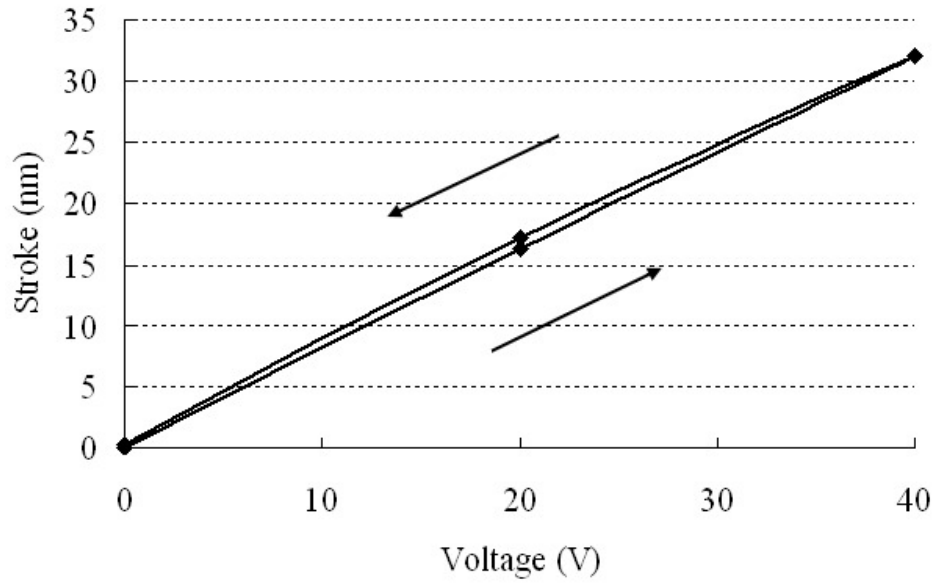
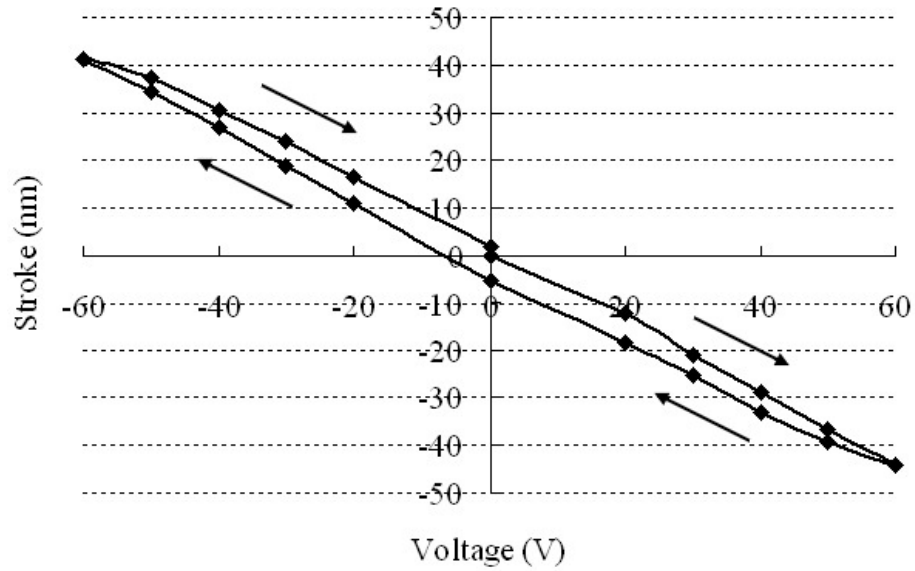
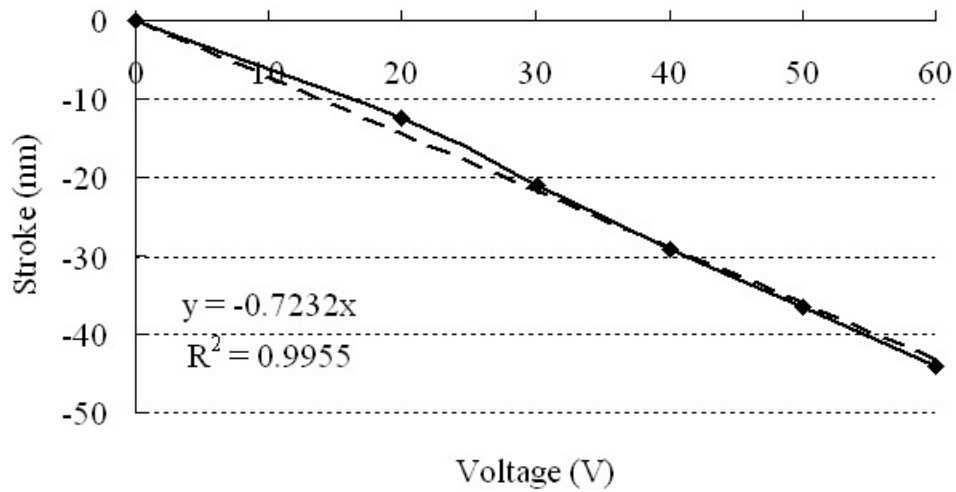


Fig. 6. The measured nonflying stroke as a function of the applied voltage for Slider #1.



(a)



(b)

Fig. 7. The measured nonflying stroke as a function of the applied voltage. (a) The voltage was gradually increased from 0 to 60 V, returned to 0 V, decreased to -60 V and returned to 0 V; (b) A linear fit of a rate of 0.72 nm/V is found to fit the measurement data from 0 to 60 V. The minus sign indicates that a negative voltage is required for a positive stroke in the actuated side-pads scheme.

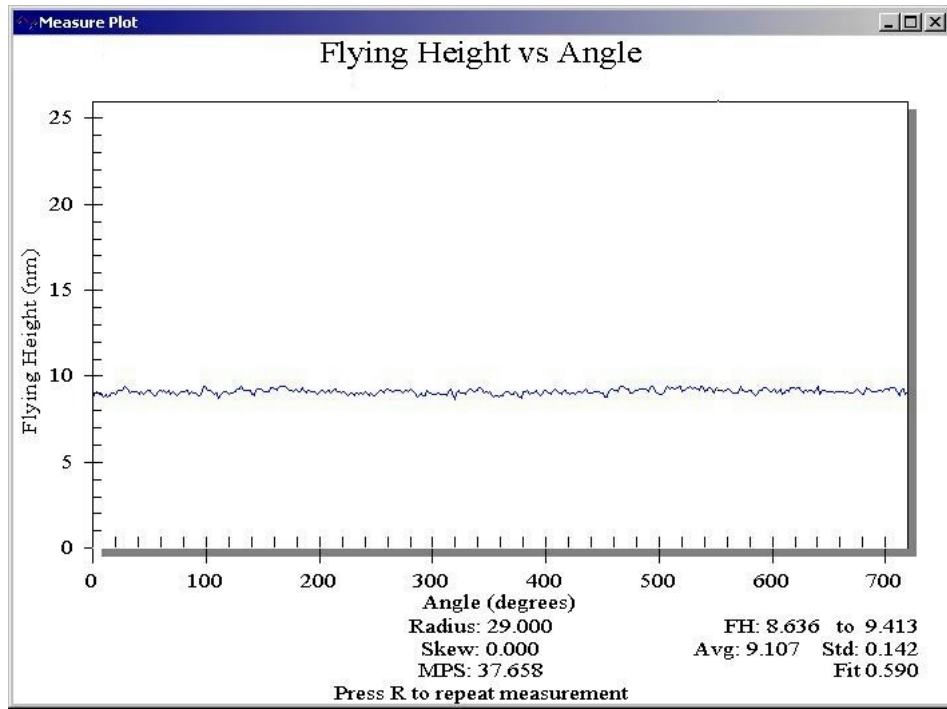
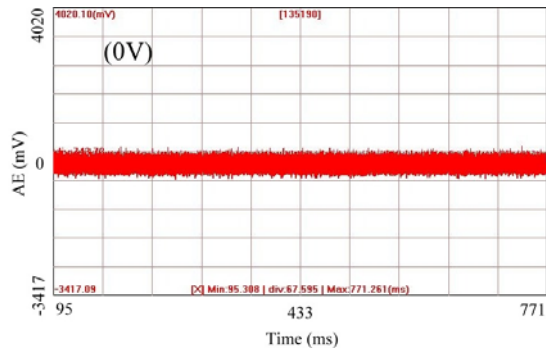
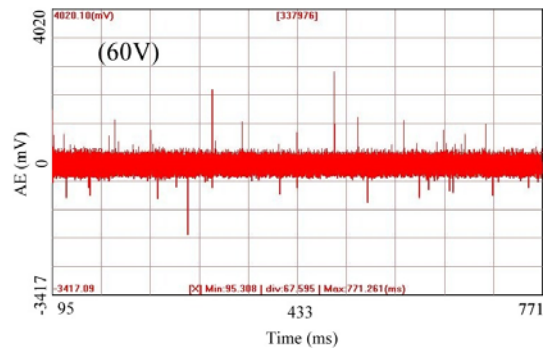


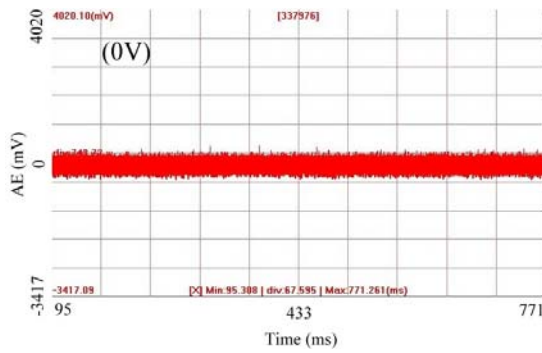
Fig. 8. The measured FH at Point A (the inner trailing pad) at the MD as a function of degree.



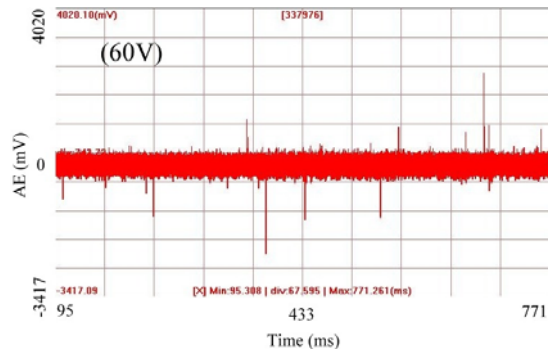
(a) Radial position: 26 mm



(b) Radial position: 26 mm

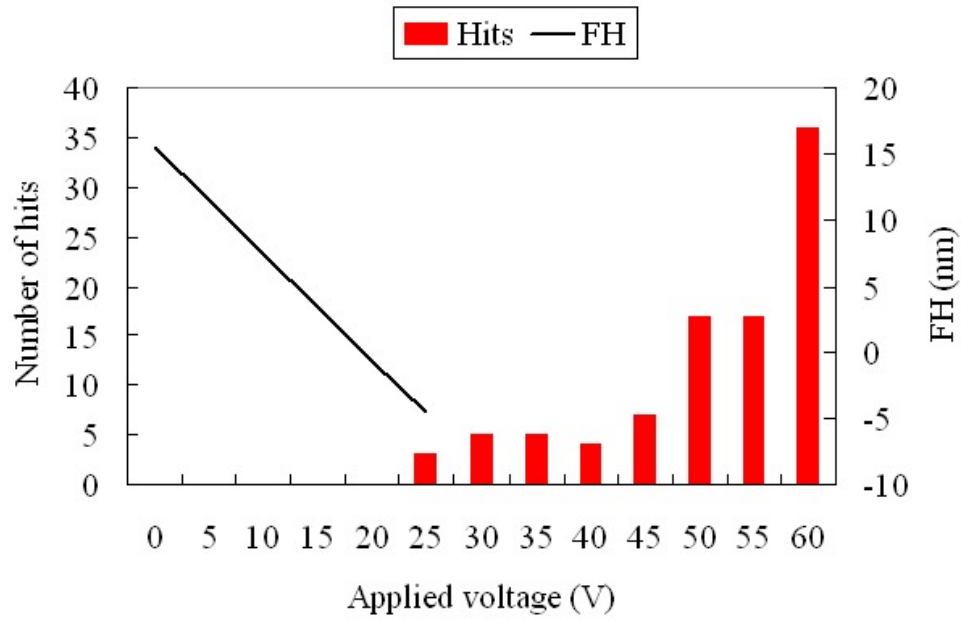


(c) Radial position: 25 mm

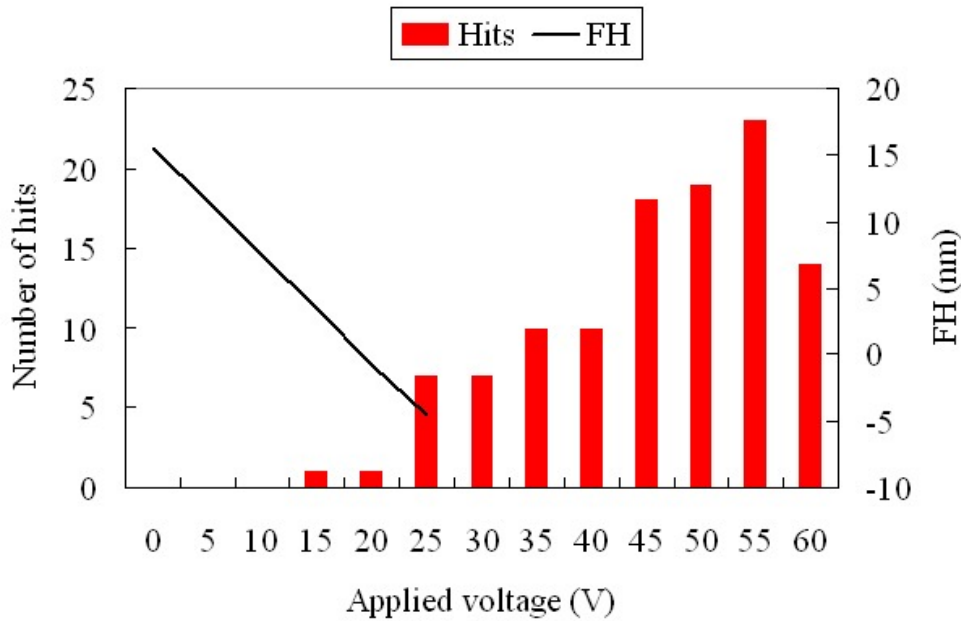


(d) Radial position: 25 mm

Fig. 9. The time histories of the AE signals: (a) 0 V at 26 mm; (b) 60 V at 26 mm; (c) 0 V at 25 mm; (d) 60 V at 25mm.



(a) Radial position: 26 mm



(b) Radial position: 25 mm

Fig. 10. The number of hits (spikes) and the estimated FH as functions of the applied voltage. The contact event that has an AE amplitude over ± 500 mV was counted as a hit.

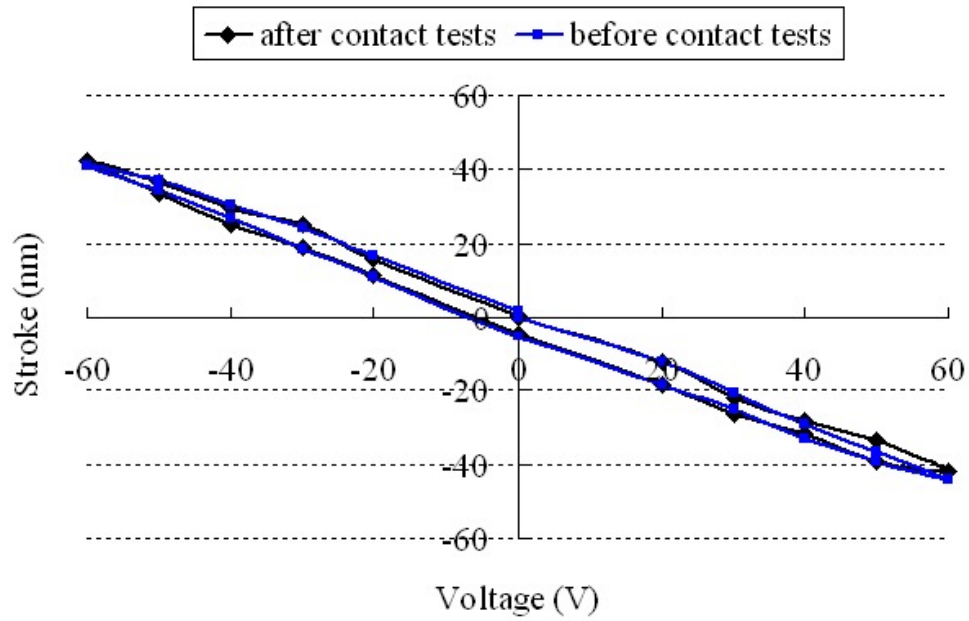


Fig. 11. Comparison of the nonflying actuated strokes measured before and after the contact test, which demonstrated good repeatability.

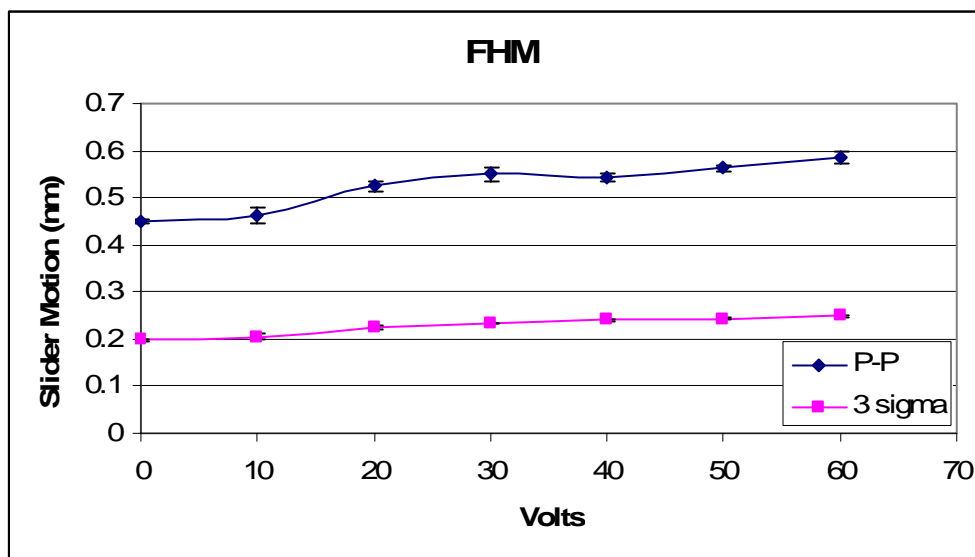


Fig. 12. Peak-to-peak and standard deviation (3σ) of slider displacements as a function of applied voltage.

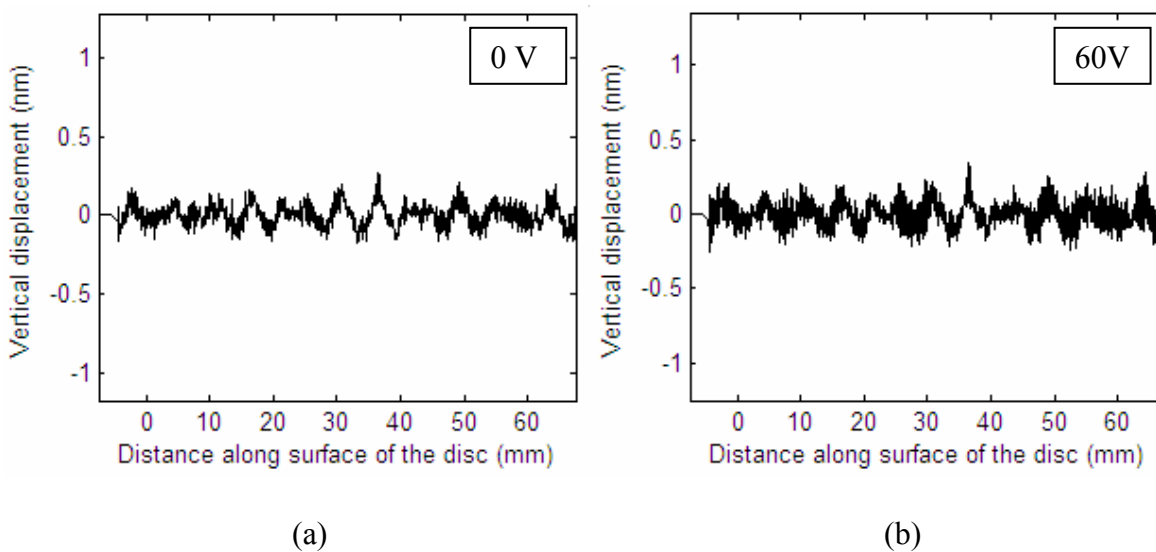


Fig. 13. Repeatable part of slider displacements: (a) when no slider-disk contact occurs; (b) when slider-disk contact occurs.

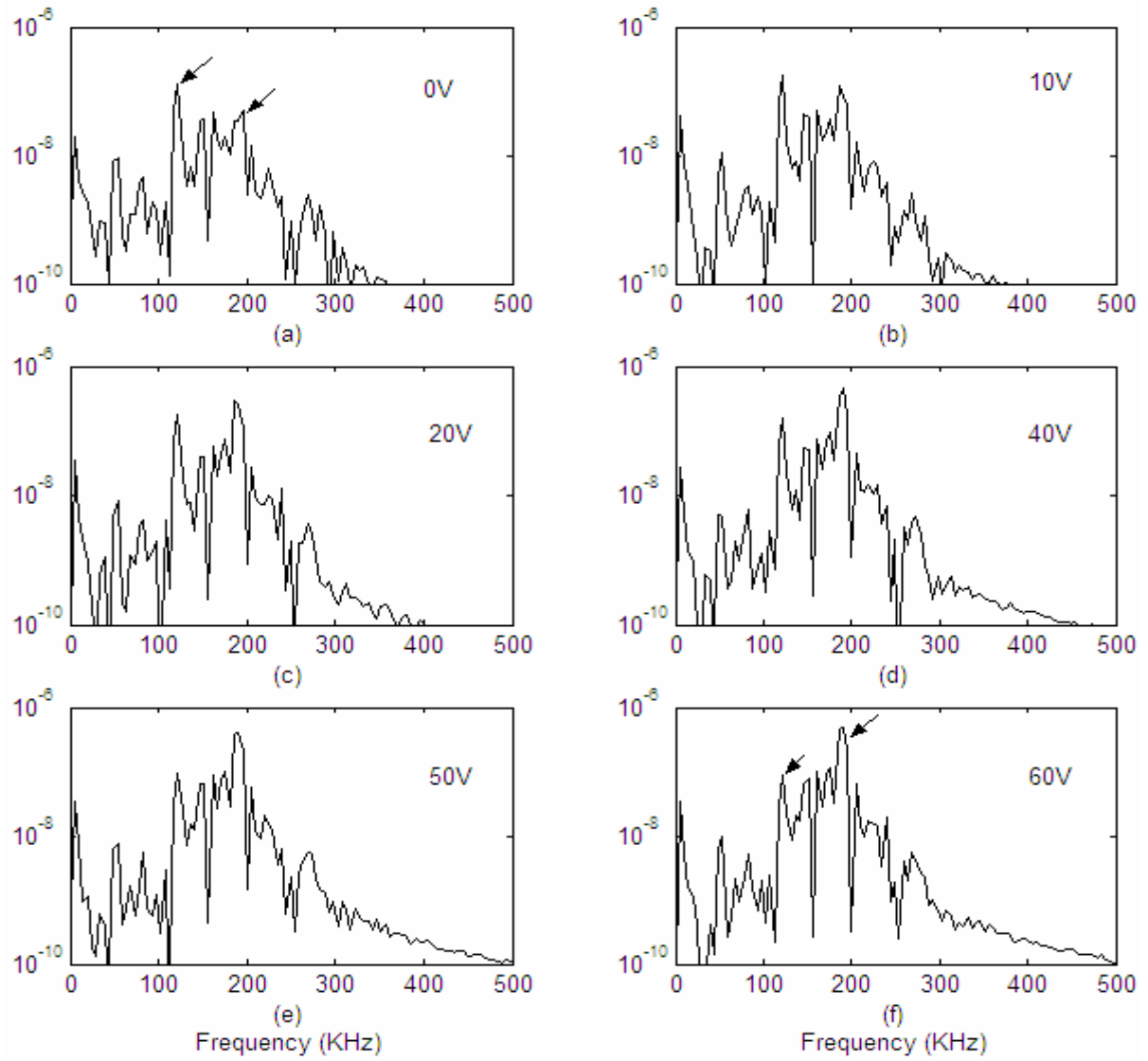


Fig. 14. Shift in the frequency response due to change in intensity of contact.

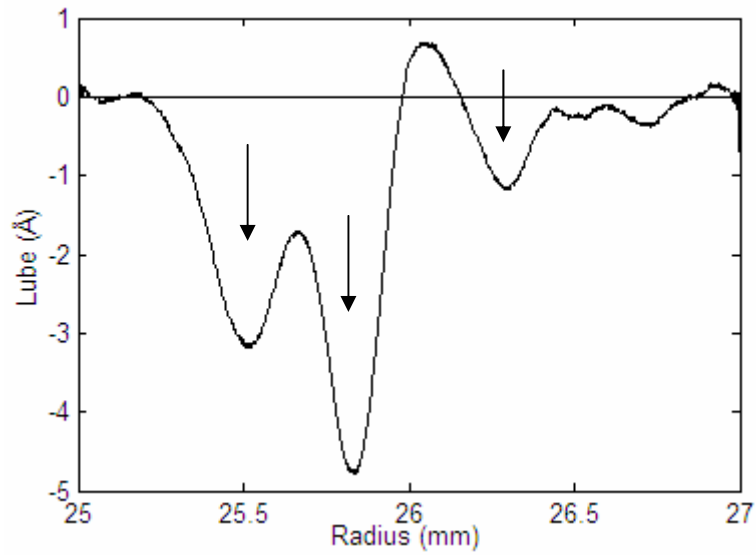


Fig. 15. Average lube height as a function of radius on an experimental track.

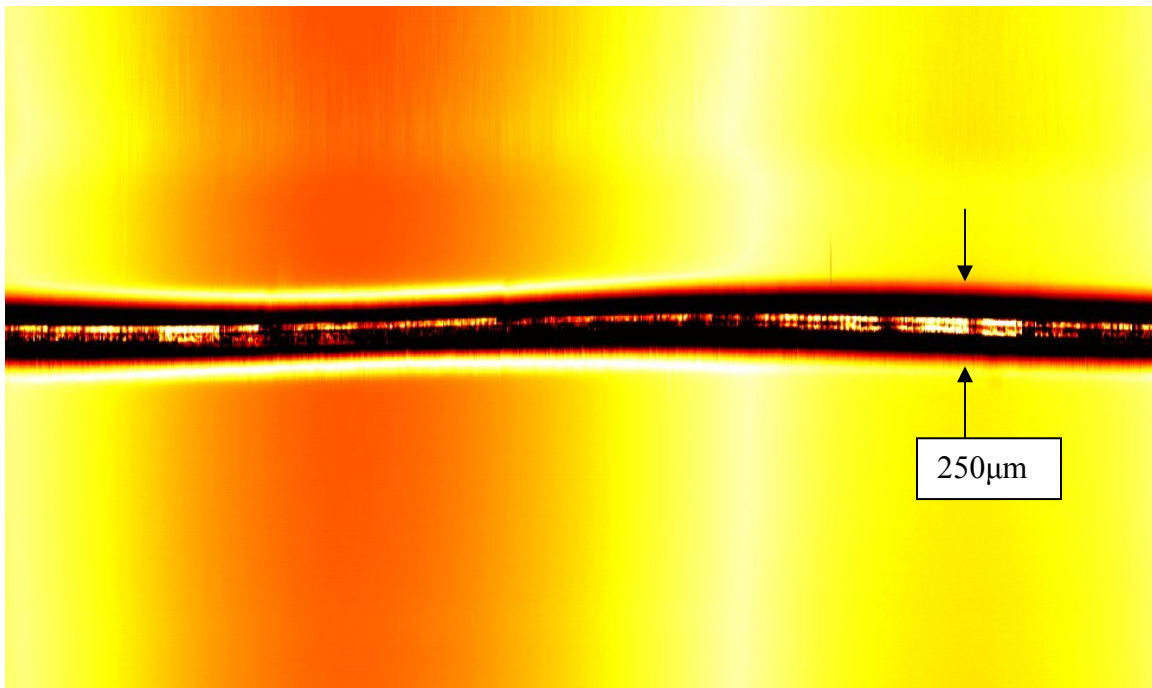


Fig. 16. OSA scan of experimental track showing lube depletion and carbon wear.

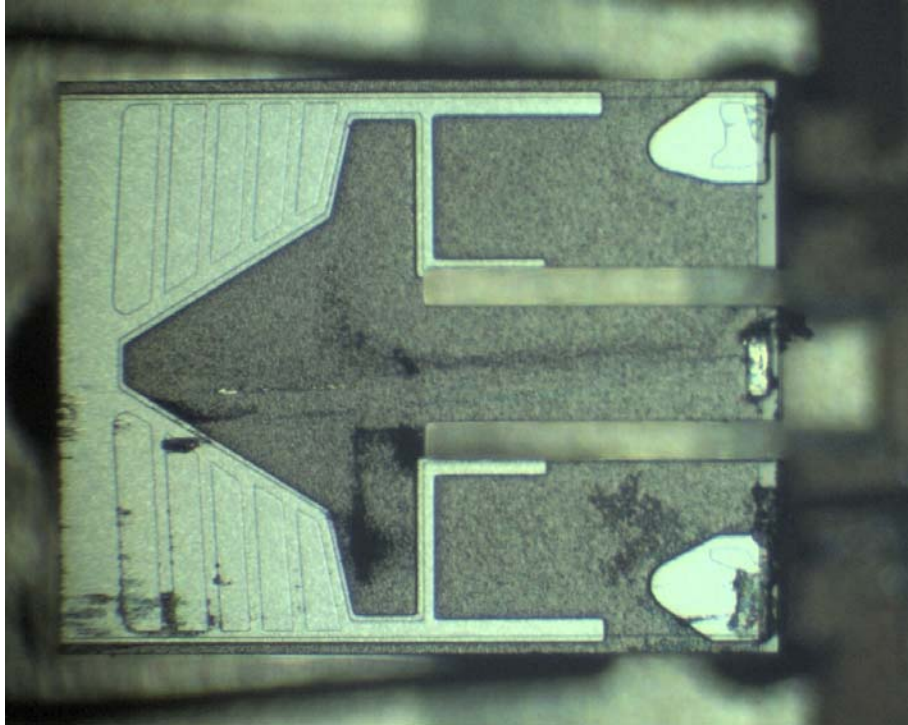


Fig. 17. Photograph of the piezoelectric slider after contact tests. Considerable amount of debris and particles were accumulated on the ABS, especially near the center and inner trailing pads.